

Antimicrobial and Antibiofilm Properties of Fluorinated Polymers with Embedded Functionalized Nanodiamonds

Nunes-Pereira, João; Costa, Pedro; Fernandes, Liliana; Carvalho, Estela O.; Fernandes, Margarida M.; Carabineiro, Sónia A.C.; Buijnsters, Josephus G.; Tubio, Carmen R.; Lanceros-Mendez, Senentxu

DOI

[10.1021/acsapm.0c00869](https://doi.org/10.1021/acsapm.0c00869)

Publication date

2020

Document Version

Accepted author manuscript

Published in

ACS Applied Polymer Materials

Citation (APA)

Nunes-Pereira, J., Costa, P., Fernandes, L., Carvalho, E. O., Fernandes, M. M., Carabineiro, S. A. C., Buijnsters, J. G., Tubio, C. R., & Lanceros-Mendez, S. (2020). Antimicrobial and Antibiofilm Properties of Fluorinated Polymers with Embedded Functionalized Nanodiamonds. *ACS Applied Polymer Materials*, 2(11), 5014-5024. <https://doi.org/10.1021/acsapm.0c00869>

Important note

To cite this publication, please use the final published version (if applicable).
Please check the document version above.

Copyright

Other than for strictly personal use, it is not permitted to download, forward or distribute the text or part of it, without the consent of the author(s) and/or copyright holder(s), unless the work is under an open content license such as Creative Commons.

Takedown policy

Please contact us and provide details if you believe this document breaches copyrights.
We will remove access to the work immediately and investigate your claim.

Article

Antimicrobial and antibiofilm properties of fluorinated polymers with embedded functionalized nanodiamonds

João Nunes-Pereira, Pedro Costa, Liliana Fernandes, Estela O. Carvalho, Margarida M. Fernandes, Sónia A. C. Carabineiro, Josephus Gerardus Buijnsters, Carmen R Tubio, and Senentxu Lanceros-Méndez

ACS Appl. Polym. Mater., **Just Accepted Manuscript** • DOI: 10.1021/acsapm.0c00869 • Publication Date (Web): 29 Sep 2020

Downloaded from pubs.acs.org on October 7, 2020

Just Accepted

"Just Accepted" manuscripts have been peer-reviewed and accepted for publication. They are posted online prior to technical editing, formatting for publication and author proofing. The American Chemical Society provides "Just Accepted" as a service to the research community to expedite the dissemination of scientific material as soon as possible after acceptance. "Just Accepted" manuscripts appear in full in PDF format accompanied by an HTML abstract. "Just Accepted" manuscripts have been fully peer reviewed, but should not be considered the official version of record. They are citable by the Digital Object Identifier (DOI®). "Just Accepted" is an optional service offered to authors. Therefore, the "Just Accepted" Web site may not include all articles that will be published in the journal. After a manuscript is technically edited and formatted, it will be removed from the "Just Accepted" Web site and published as an ASAP article. Note that technical editing may introduce minor changes to the manuscript text and/or graphics which could affect content, and all legal disclaimers and ethical guidelines that apply to the journal pertain. ACS cannot be held responsible for errors or consequences arising from the use of information contained in these "Just Accepted" manuscripts.

Antimicrobial and antibiofilm properties of fluorinated polymers with embedded functionalized nanodiamonds

João Nunes-Pereira^{†,‡,}, Pedro Costa^{‡,#}, Liliana Fernandes[‡], Estela O. Carvalho^{‡,‡},*

Margarida M. Fernandes^{‡,‡}, Sónia A.C. Carabineiro[‡], Josephus G. Buijnsters[‡],

Carmen R. Tubio[§], and Senentxu Lanceros-Mendez^{§,‡,}*

[†] Centre for Mechanical and Aerospace Science and Technologies (C-MAST),

Universidade da Beira Interior, Rua Marquês d'Ávila e Bolama, 6200-001 Covilhã,

Portugal

[‡] Centro de Física das Universidades do Minho e do Porto (CF-UM-UP), Campus de

Gualtar, 4710-057 Braga, Portugal

[#] Institute for Polymers and Composites IPC/I3N, University of Minho, 4800-058

Guimarães, Portugal

[‡] Centre of Biological Engineering, University of Minho, Campus de Gualtar, 4710-

057 Braga, Portugal

[‡] LAQV-REQUIMTE, Department of Chemistry, NOVA School of Science and Technology, Universidade NOVA de Lisboa, 2829-516 Caparica, Portugal

[‡] Department of Precision and Microsystems Engineering, Micro and Nano Engineering, Delft University of Technology, 2628 CD Delft, The Netherlands

[§] BCMaterials, Basque Center for Materials, Applications and Nanostructures, UPV/EHU Science Park, 48940 Leioa, Spain.

[±] IKERBASQUE, Basque Foundation for Science, 48009 Bilbao, Spain

KEYWORDS

Nanodiamonds; Poly(vinylidene fluoride); Solvent casting; Polymer composites; Antimicrobial films.

ABSTRACT

1
2
3 Environmentally resilient antimicrobial coatings are becoming increasingly required for
4
5
6
7 a wide range of applications. For this purpose, nanocomposite thin films of
8
9
10 poly(vinylidene fluoride) (PVDF) filled with several types of functionalized
11
12
13 nanodiamonds (NDs) were processed by solvent casting. The effects of ND inclusion
14
15
16 and functionalization in their morphological, structural, optical, thermal and electrical
17
18
19 properties were evaluated taking into account the type of the nanofiller and a
20
21
22 concentration up to 2 wt.%. The morphology, structure and thermal features of the
23
24
25 polymer matrix are governed by the processing conditions and no noticeable changes
26
27
28 occurred due to the presence of the ND fillers. The polymer crystallized mainly in the
29
30
31 α phase with a crystallinity of $\approx 60\%$. In turn, the optical transmittance from 200 to 800
32
33
34 nm and the dielectric constant effectively depended on the ND type and content. The
35
36
37 inclusion of the ND particles effectively provided antimicrobial properties to the films,
38
39
40
41 which depended on the ND functionalization. This study thus shows that the
42
43
44 incorporation of functionalized NDs into PVDF allows the development of antimicrobial
45
46
47 coatings with tailorable optical and dielectric properties, which could be of great
48
49
50 importance to face nowadays pandemic crisis scenario.
51
52
53
54
55
56
57
58
59
60

INTRODUCTION

Polymer composite science and technology is a rapidly increasing field of research, mostly due to the possibilities on tailoring materials functional properties for application in a large variety of areas. The introduction of small amounts of a nanomaterial within a polymeric matrix can lead to large enhancements to its features, such as optical, mechanical, electrical and thermal properties ¹⁻².

Furthermore, new functional properties can be added otherwise not existing in the polymer matrix, such as magnetic ³ or photochromic ⁴ response, among others. Other properties that can be added and/or enhanced are those related to the applicability of the materials as coatings, such as tailored hydrophobicity ⁵, self-cleaning ⁶ or antimicrobial features ⁷.

Among the many nanomaterials synthesized in recent years, nanocarbons have been intensively used for several purposes. In particular, diamond nanostructures (nanodiamonds, NDs) were synthesized for the first time in the 1960s and remained practically unexplored until the 1990s when important breakthroughs led to an

1
2
3 increasing interest in the applications of these nanostructures. NDs present
4
5
6
7 enhanced mechanical properties (including Young's modulus and hardness),
8
9
10 elevated electrical resistivity and thermal conductivity (up to about 2000 W/m.K), high
11
12
13 surface area with tunable surface structure, optical properties such as fluorescence
14
15
16 (nitrogen-vacancy centers) and photoluminescence. Further, they are biocompatible,
17
18
19 chemically stable and resistant to severe environment conditions, and offer the
20
21
22 possibility to attach different functional groups to their surface without losing the main
23
24
25 features of the diamond core ⁸⁻¹⁰. Thus, the aforementioned properties along with the
26
27
28 rich chemistry of the surface, make NDs excellent nanostructures to developing
29
30
31 polymer composites and, nowadays, NDs are being explored for a large number of
32
33
34 applications, such as drug delivery, cancer therapy, biosensors, surgical implants,
35
36
37 tissue engineering, biomedical imaging, tribology and lubrication, and antimicrobial
38
39
40 applications ^{8, 11-12}. Yet, other materials composed by nanostructures of carbon, e.g.
41
42
43 carbon nanotubes, fullerene, diamond-like carbon and graphene demonstrated to
44
45
46 have a wide spectrum of antibacterial activities for different pathogens ¹³. As such,
47
48
49 they have been investigated as fillers in polymeric matrices for developing materials
50
51
52 displaying antifouling, antibiofilm and antimicrobial properties ¹⁴ in a similar approach
53
54
55
56
57
58
59
60

1
2
3 to other antimicrobial materials comprising nanostructures. Standard antibacterial
4
5
6
7 coatings or surfaces are usually produced by incorporating antimicrobial agents, such
8
9
10 as copper and copper alloys ¹⁵, silver compounds ¹⁶, or organic molecules containing
11
12
13 quaternary ammonium chemical groups ¹⁷. However, concerns about the cytotoxicity
14
15
16
17 of these nanoparticles against human cells have been expressed ¹⁸⁻¹⁹.

18
19
20
21 Due to their biocompatibility, tailorable surface chemistry and large surface area, NDs
22
23
24
25 have already been studied for non-toxic antimicrobial/antifungal materials ²⁰, as well
26
27
28 as for other applications like adsorption and controlled release of anti-cancer drugs,
29
30
31
32 such as 4-hydroxytamoxifen ²¹, paclitaxel ²² and tetracyclines ²³⁻²⁴. Combining the
33
34
35 attachment of specific drugs to the ND surface with controlled release, provides a
36
37
38
39 new opportunity for anticancer chemotherapeutics. Its elevated hardness, Young's
40
41
42 modulus, rich chemistry of the surface and chemical properties make the core of NDs
43
44
45 suitable to enhance the mechanical and chemical properties of bioresorbable
46
47
48
49 polymer scaffolds for tissue engineering, as demonstrated in PLGA (poly(lactic-*co*-
50
51
52 glycolic acid)) filled with phospholipid ND compound (NDPC), which has been
53
54
55
56
57 successfully evaluated for bone tissue engineering *in vivo* and *in vitro* ²⁵. ND particles
58
59
60

are also stable in aqueous media making them suitable to use in the design of modified electrodes and a promising material for electrochemical sensors with high analytical performance ²⁶.

With the introduction of NDs to polymeric matrices, the composites obtained have superior thermal, mechanical and optical properties that combined with the biocompatibility and chemical stability of the NDs provide important options for biomedical applications ^{8, 27}. Among the broad range of polymer matrices able to be combined with ND fillers, PVDF (poly(vinylidene fluoride)) and copolymers are an attractive choice in the case of multifunctional polymer coatings due to their remarkable electroactive characteristics, namely pyro, piezo and ferroelectric effects, what makes them a suitable choice to develop advanced and functional materials , including sensors and actuators ^{12, 28}. PVDF can crystallize in five distinct phases, α , β and γ being the most common. This polymer has some outstanding features such as high chemical and UV resistances, mechanical strength, hydrophobicity, thermal stability and flexibility compared to several commercial polymeric materials, which drives the manufacture of new PVDF based nanocomposites for technological

1
2
3 applications²⁸⁻²⁹. The electroactive properties of PVDF have been used to develop
4
5
6
7 new strategies for tailoring bacterial behaviour, either growth or inhibition of
8
9
10 *Staphylococcus epidermidis* and *Escherichia coli*, mainly when mechanically
11
12
13
14 stimulated³⁰. This study reports the production of ND/PVDF composites by a solvent
15
16
17 casting. It is worth noting that solvent casting approaches are gaining increasing
18
19
20 interest as they allow processing by additive manufacturing fabrication processes,
21
22
23
24 such as spray, screen or even ink-jet printing³¹, suitable for the implementation of
25
26
27 coatings and devices. The morphology, structural, optical, thermal and electrical
28
29
30 properties of the ND/PVDF composite films were evaluated, as well as their
31
32
33
34 antimicrobial characteristics, which proved to be suitable to develop antiseptic
35
36
37
38 materials of high interest to deal with pandemic crises, in order to avoid bacterial co-
39
40
41 infections. In fact, serious secondary bacterial infections are considered an important
42
43
44
45 complication of SARS-CoV-2 virus infection (COVID-19)³².
46
47
48
49
50
51
52
53

54 EXPERIMENTAL DETAILS

55
56
57
58
59
60

Materials. PVDF (Solef 1010) was obtained from Solvay. DMF (*N,N*-dimethylformamide, 99.5%) solvent was acquired from Fluka. Carbodeon uDiamond® Molto (non-functionalized ND, hereafter denoted as NDM), with 5 nm average particle size was obtained from Carbodeon Ltd Oy, Vantaa (Finland). Functionalized samples, namely uDiamond® VOX P (carboxyl monofunctionalized, hereafter denoted as NDO), uDiamond® Amine P (amine monofunctionalized, hereafter denoted as NDA) and uDiamond® Hydrogen P (hydrogen monofunctionalized, hereafter denoted as NDH), were also obtained from the same supplier.

Sample preparation. The ND/PVDF based composites followed a typical solvent casting method using doctor blade technique ²⁹. Initially, the ND particles were dispersed in DMF and placed in an ultrasound bath for 4 h. The PVDF powder was added to the solution at a ratio of 10/90 wt.% of PVDF/DMF and the relative concentration of the ND fillers to polymer varied between 0.25 and 2 wt.%. The solution was magnetically stirred at 40 °C, until the PVDF completely dissolved, and

then spread with a bar coater on top of a clean glass substrate. Solvent evaporation was performed at 210 °C (above the melting temperature of PVDF) in an oven (Binder, ED23) to obtain composite films with a thickness of 20 to 25 µm and a compact morphology to evaluate the effect of nanofillers-polymer interactions in the crystallization of the composites, as these processing conditions lead to preferential crystallization in the α phase of PVDF ²⁹. Hereafter, the polymer composites will be identified by the ND nanoparticles functionalization type (NDM, NDA, NDO and NDH, respectively) and the respective nanofiller amount (in wt.%).

Sample characterization. Surface element quantification of the ND/PVDF composites was carried out by X-ray photoelectron spectroscopy (XPS, Kratos AXIS Ultra HSA spectrometer). It was used a monochromatic Al K α X-ray source (1486.7 eV) in fixed analyzer transmission (FAT) mode at 15 kV (90 W), with 40 eV of pass energy for regions ROI and a survey of 80 eV. Charge neutralization system was used to acquire data at a pressure $<1 \times 10^{-6}$ Pa. Survey and multi-region spectra were obtained for C1s, O1s and N1s peaks, and the values of binding energy were referred to the C1s peak at 284.6 eV. The obtained spectra were fitted to Gaussian

and Lorentzian curves with CASA XPS software after a Shirley background subtraction.

The nanoparticles distribution and composites morphology were analyzed by SEM (scanning electron microscopy, NanoSEM - FEI Nova 200 (FEG/SEM)), with 15 kV of accelerating voltage. Prior evaluation, a thin layer of gold (20 nm) was deposited on the samples by magnetron sputtering (Polaron SC502).

AFM (atomic force microscopy, CSInstruments set-up) was performed to study the surface roughness of the samples. Measurements were performed in squares with 20×20 μm in the non-contact resonant mode (73 kHz of frequency and 84° of amplitude) to avoid samples damage and AFM tangling.

The surface wettability was studied by contact angle measured in a Dataphysics system OCA20 at room temperature with ultrapure water (5 μL) in different spots for each sample. The SCA20 software allowed to determine the contact angle and the results are presented as an average of 6 measurements per sample with the respective standard deviation (SD).

The UV-Vis spectroscopy experiments (Jasco V-670 spectrophotometer) were performed at room temperature to study the optical characteristics of the composites, within the range of 200 to 900 nm.

Fourier-transform infrared spectroscopy (FTIR) in attenuated total reflectance (ATR) mode (Jasco FT/IR-4100) was performed to study the polymer phase in the composites. 32 scans with a resolution of 4 cm⁻¹ were carried out in the range of 4000 to 600 cm⁻¹. Considering that the polymer crystallizes mainly in the α or β phases, the α PVDF relative content ($F(\alpha)$) was calculated considering the absorbance at 766 cm⁻¹ (A_α) and 840 cm⁻¹ (A_β), and the absorption coefficients at the correspondent wavenumber ($K_\alpha = 6.1 \times 10^4$ cm².mol⁻¹; $K_\beta = 7.7 \times 10^4$ cm².mol⁻¹) after equation 1 ²⁸:

$$F(\alpha) = \frac{A_\alpha}{\left(\frac{K_\alpha}{K_\beta}\right)A_\beta + A_\alpha} \quad (1)$$

The thermal properties of the composites were analyzed by DSC (differential scanning calorimetry) thermography (Perkin-Elmer DSC 8000). The measurements were performed at a heating rate of 10 °C/min, under flowing nitrogen atmosphere, in the range of 25 to 250 °C. 30 μ L perforated aluminium pans were used to release

1
2
3 volatiles. The degree of crystallinity (χ_c) was determined by the melting enthalpy of
4
5
6
7 the sample (ΔH_f) and the melting enthalpy of PVDF 100 % crystalline (ΔH_{100} , 104.6
8
9
10 J/g) through the equation 2 ³³:

$$\chi_c = \frac{\Delta H_f}{\Delta H_{100}} \quad (2)$$

11
12
13
14
15
16
17
18
19 Prior to the electrical characterization circular gold electrodes (5 mm diameter) were
20
21
22
23 deposited on both film sides by sputtering (Polaron SC502 sputter coater) under the
24
25
26 following conditions: 3×30 s at ≈20 mbar and ≈20 mA.
27
28

29
30 The dielectric analysis was performed measuring the capacity (C) and the dielectric
31
32
33
34 loss ($\tan(\delta)$) at room temperature with a LCR meter (Quadtech 1920) applying a
35
36
37
38 signal voltage of 1.0 V sweeping the frequency from 500 Hz to 1 MHz. To calculate
39
40
41 the dielectric constant (ϵ') the geometrical parameters (error of ≈1 %) of the parallel
42
43
44
45 plate capacitor.
46
47

48
49 The a.c. conductivity (σ') was calculated from dielectric measurements through the
50
51
52
53 angular frequency (ω), the permittivity of the free space (ϵ_0) and the imaginary part of
54
55
56 ϵ' dependent of frequency (ϵ'') by equation 3:
57
58
59
60

$$\sigma' = \omega \epsilon_0 \epsilon'' \quad (3)$$

The d.c. electrical conductivity (σ) was determined, after obtaining the d.c. volumetric electrical resistivity (ρ_v) from the characteristic IV curves obtained with a picoammeter/voltage source (Keithley 487), through the the electrical resistance (R), the sample thickness (L) and electrodes area (A) by equation 4:

$$\frac{1}{\sigma} = \rho_v = R \frac{L}{A} \quad (4)$$

Antimicrobial and antibiofilm activity. The inhibition of bacterial growth was assessed against a Gram-negative, *Escherichia coli* (*E. coli*) strain ATCC® 8739™ acquired to American Type Culture Collection (LGC Standards S.L.U, Spain). To prepare the bacterial inoculum, a single colony was isolated from an agar plate and grown in Nutrient Broth (NB, Dehydrated Culture Media, Panreac) overnight, at 37 °C and 110 rpm, until the stationary phase was reached. The bacteria cell population was estimated using spectrophotometer optical density (OD) readings at 600 nm and adjusted as required in each experiment. This process was performed for all bacteria assays.

Nanodiamonds bacteriostatic activity. Bacteria susceptibility to the non-functionalized and different functionalized NDs was measured in suspension through a microdilution assay performed in NB. Succinctly, various concentrations of NDs working solutions were prepared by performing ten-fold serial dilutions, of a starting solution of 0.16 mg.mL^{-1} . A 96-well polystyrene plate was filled with $75 \text{ }\mu\text{L}$ of NDs diluted solutions and $75 \text{ }\mu\text{L}$ of bacteria inoculum, obtaining the final concentration of $5 \times 10^5 \text{ CFU (colony forming units) mL}^{-1}$. The bacteria growth was assessed after 24 h, through OD measurements at 600 nm with a microplate reader (Biotek Cytation3). The reported growth inhibition rates were the mean values of 4 independent experiments with the respective SD.

Films bacteriostatic activity. *E. coli* bacteriostatic activity assessed in contact with the processed ND/PVDF composite films was evaluated. First, the films were cut into disks of 13 mm diameter, sterilized and placed on 24-well nontreated polystyrene plates. A bacterial inoculum of $5 \times 10^5 \text{ CFU.mL}^{-1}$ was incubated overnight at a temperature of $37 \text{ }^{\circ}\text{C}$. The bacterial cultures were further diluted in phosphate buffer solution (PBS) and plated ($100 \text{ }\mu\text{L}$) on a NB agar plate and incubated at $37 \text{ }^{\circ}\text{C}$. After

24 h, the number of CFUs was determined, which allowed the quantification of viable bacteria present on the inoculated solution. Five independent assays were performed and bacterial cells incubated only with NB was used as a control

Biofilm inhibition test. The quantification of biofilm total biomass, growing over the materials, was evaluated using crystal violet assay. For optimal biofilm growth, a concentration of 5×10^6 CFU.mL⁻¹ *E. coli* inoculum was grown above the sterilized films on 24-well nontreated polystyrene plates, during 24 h at 37 °C. Then, the medium was discarded, and biofilms washed with sterile PBS. This process was repeated for three times to exclude non-adhered bacteria. Biofilms were further fixed using heat (60 °C) for 60 min. A solution of 0.1% (w/v) in PBS crystal violet solution and incubated for 10 min at RT. Crystal violet was removed and samples cleaned with distilled water, for three times. The residual stain was diluted with 30% acetic acid and a microplate reader (Biotek Cytation3 was used to measure the absorbance at 595 nm). PVDF 1010 films were used as control sample, where cells adhered at certain extent and formed a biofilm.

Live/Dead Kit. The bacteria growing on the materials was further visualized under fluorescence microscope after live/dead staining using LIVE/DEAD™ BacLight™ Bacterial Viability Kit, for microscopy (Invitrogen, US). *E. coli* was grown for 24 h on 24-well nontreated polystyrene plates over the sterilized films at 37 °C. Then, the samples were washed twice with PBS. The adhered cells were stained in dark conditions for 15 min with 0.1% (v/v) SYTO9 and 0.1% (v/v) propidium iodide. The samples were then visualized in a fluorescence microscope (Olympus BX51 microscope) and the obtained fields were captured using a magnification of 40 X.

RESULTS AND DISCUSSION

Chemical analysis of nanodiamond fillers. Figure 1 shows the XPS results of the ND samples. The C1s peak around 286 eV (Figures 1a, d, g and j) is assigned to sp^3 bonded carbon (C–C) and the peak at ≈ 284.6 eV refers to sp^2 carbons (C=C) associated to specific defects in the surface of the NDs ³⁴. The peaks at around 287 eV (C–O) and 288 eV (C=O) deal with ND oxygenated surface groups.

The O1s spectra (Figures 1b,e,h,k) were deconvoluted in three peaks attributed to C=O (529 eV), C–O (1) in ether, alcohol and epoxy groups (530 eV) and C–O (2) in ester and carboxyl groups (532 eV). The oxygen content on the surface of the samples followed the order NDO > NDM > NDA > NDH, with the NDO sample (carboxylated) showing the highest oxygen content (9.5%), as expected, due to several oxygenated groups, as previously reported for samples thermally oxidized in air ³⁵. Non-functionalized ND (NDM) also showed a high oxygen content (6.3%), as a result of its production and purification procedures ³⁶, i.e. detonation with the explosive precursors 1,3,5-Trinitroperhydro-1,3,5-triazine and 2,4,6-Trinitrotoluene followed by a treatment with boiling acid to remove the impurities and the amorphous carbon resulting from the soot of detonation. The XPS results show that the treatments for hydrogenation and amination to obtain NDA and NDH materials, resulted in the removal of most of the oxygenated groups from the surface, thereby reducing the oxygen concentration about 2%.

The XPS profiles differ in the quantity of oxygenated groups in the surface and of sp^2 carbon. The lowest ratio of sp^2/sp^3 was registered in the non-functionalized NDM

composite (0.94), which shows that the functionalization treatments leads to an increase in the number of surface structural defects of NDs structure.

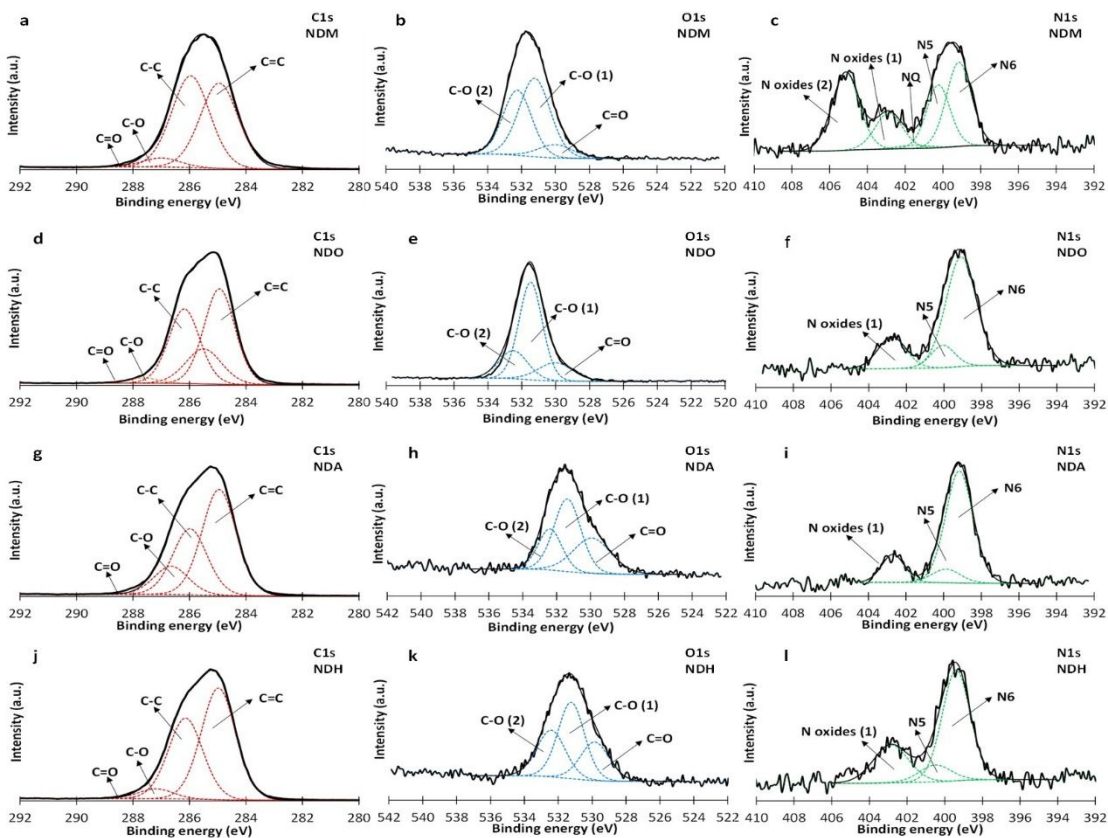


Figure 1. XPS spectra and deconvolution of C1s (a, d, g and j), O1s (b, e, h, k) and N1s (c, f, i and l) regions of the different ND samples: NDM (a-c), NDO (d-f), NDA (g-i), NDH (j-l).

The N1s XPS spectra of the ND samples (Figures 1c, f, i and l) can be deconvoluted in four components: the peak N6 is assigned to pyridinic-N groups (≈ 399 eV), the peak N5 correspond to pyrrolic-N groups (≈ 400 eV) and the peak NQ deals with quaternary nitrogen (≈ 401)³⁷; the peaks at ≈ 403 and ≈ 405 eV are linked to N oxides³⁸. The N-content of the samples differed from 1.5% to 2.1%, characteristic of NDs obtained by detonation³⁹⁻⁴¹. Nitrogen was present in the initial explosive mixture used to produce the NDs and was therefore likely incorporated into the diamond lattice^{36, 42}.

Morphology and topography. The distribution of the NDs within the PVDF and the morphology of the composites were studied by SEM (Figure 2). Given the results similarity observed through SEM micrographs, only representative images are shown.

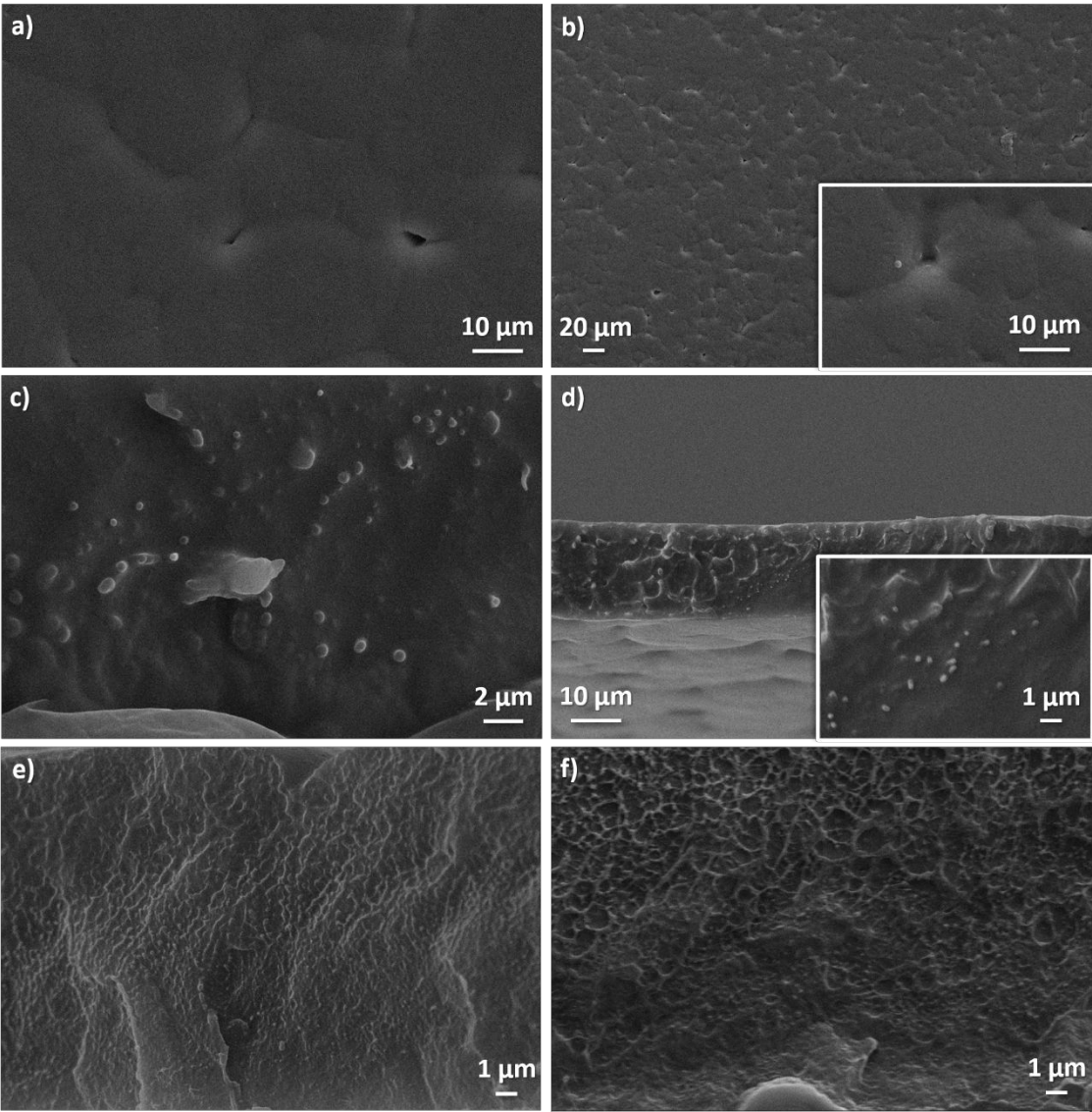


Figure 2. SEM micrographs of the surface of a) NDH 0.5 wt.%, b) NDM 2 wt.% and the cross section of c) NDO 0.5 wt.%, d) NDA 2 wt.%, e) NDH 0.25 wt.% and f) NDM 2 wt.%.

Figures 2a and 2b show the surface of the composites NDH and NDM, which is mostly regular and homogeneous throughout its extension and with the characteristic PVDF spherulitic structure. It is notorious that small pores are present between the spherulites which resulted from high temperatures (210 °C) during the polymer processing ⁴³. In the inset of Figure 2b it is possible to observe a ND aggregate near to the pore. The cross sections of the samples NDO 0.5 wt.%, NDA 2 wt.%, NDH 0.25 wt.% and NDM 2 wt.% are presented in Figures 2c to 2f. All ND filler types appear well distributed and scattered along the section of the PVDF, also presenting homogeneous sizes in a submicron range. Although, it is possible to identify some ND clusters of higher size in both samples, being more visible in the NDO sample, indicating that ND nanofillers with higher oxygen content are more difficult to disperse, similarly to what was verified in previous works ¹².

The topography of the samples was analysed by AFM measurements for pristine PVDF and samples with 2 wt.% of nanofillers content (Figure 3).

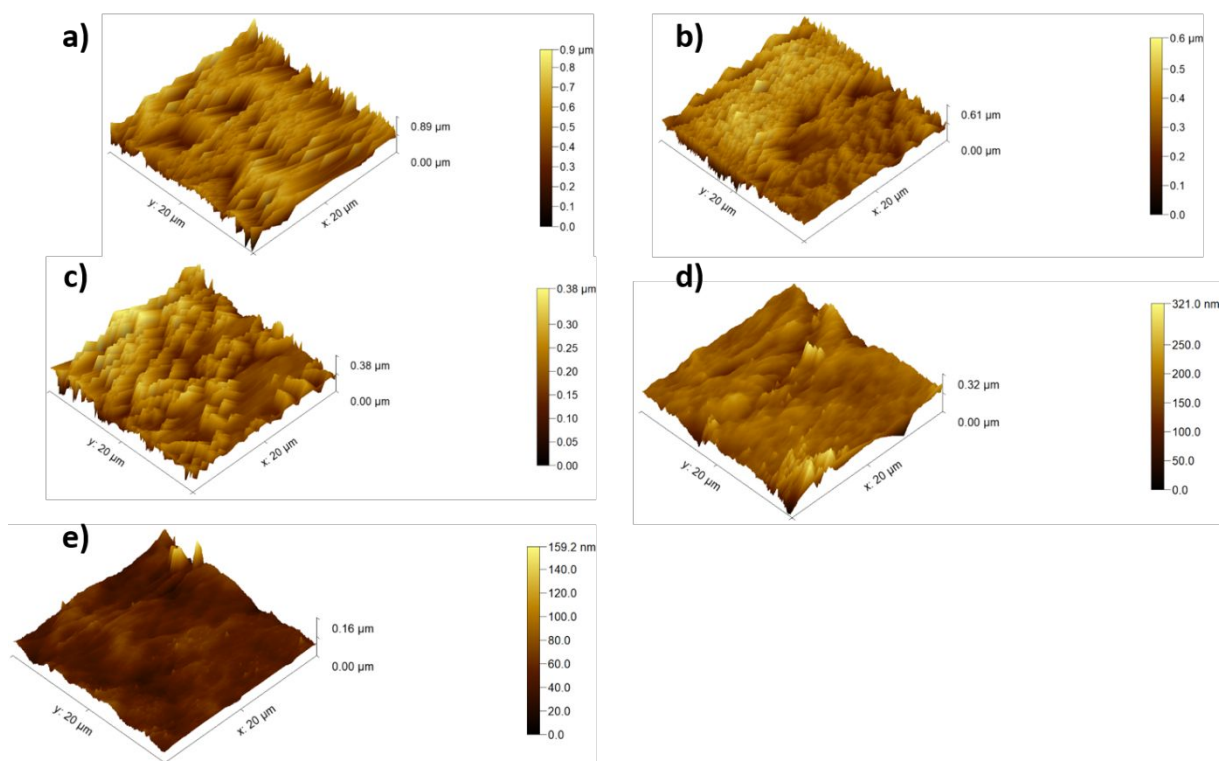


Figure 3. 3D AFM images of PVDF (a) and composites with 2 wt.% of nanofillers NDM (b), NDO (c), NDA (d) and NDH (e).

The analysis of Figure 3 shows that no relevant differences can be found between the overall topography of PVDF sample and composites. The surface of the PVDF sample shows hills and valleys characteristic of the polymer film surface⁵ and this morphology is also present in the composite samples surface. It is observed a tendency for smaller ridges compared to pristine sample indicating that the ND fillers contribute to a slight smoothing of the surface as a result of the interactions between

1
2
3 polymer and ND nanostructure. Although, the addition of the ND nanofillers do not
4
5
6
7 induce more than slight changes in the roughness (Ra) of the samples, which present
8
9
10 variations of Ra ranging between ≈ 10 to 100 nm for the NDH 2 wt.% and PVDF
11
12
13 respectively.
14
15
16
17

18 The effect of the ND nanofillers in the wettability of the composites was evaluated by
19
20
21 water contact angle and the results are presented in Figure S1. It can be seen that
22
23
24 water contact angle is not significantly influenced by the different types of NDs in the
25
26
27 polymer matrix since all of them present similar values of approximately 81° for the
28
29
30 materials with 0.25 wt.%. This was expected since AFM measurements also showed
31
32
33 similar topography and roughness among the samples. Nevertheless, by increasing
34
35
36 the content of filler from 0.25 % to 2 % the wettability is increased. While pristine
37
38
39 PVDF presents a contact angle of approximately 84° , the inclusion of the NDs
40
41
42 decrease the contact angle to values below 80° . In general, the greater the surface
43
44
45 roughness the smaller the water contact angle ⁴⁴. The inclusion of the particles
46
47
48 induces an even more uneven surface thus increasing wettability.
49
50
51
52
53
54
55
56
57
58
59
60

Optical, structural and thermal properties. In Figure 4 is shown the UV-Vis spectra of the PVDF pristine polymer and ND/PVDF composites (Figure 4a) and the dependence of the absorbance of the nanocomposite films with ND fillers concentration and type (Figure 4b).

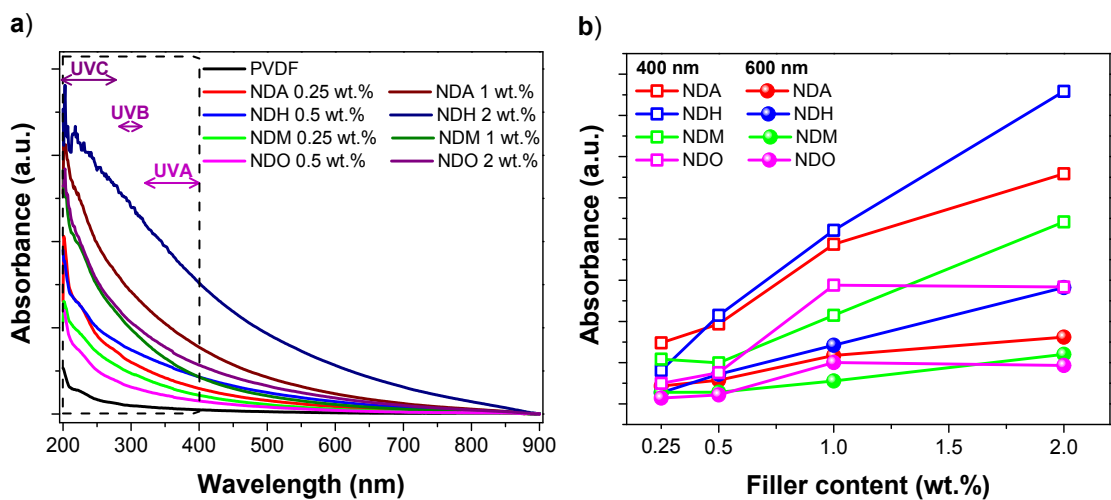


Figure 4. a) UV-Vis absorbance spectra of pristine PVDF and various ND/PVDF composite films; b) optical absorbance as a function of ND content and type.

By analyzing the UV-Vis spectra of the PVDF composite films with embedded NDA, NDH, NDM and NDO between 200 and 800 nm (Figure 4a) it is verified that the ability of the nanocomposites in absorbing UV radiation increased with the presence

and weight content of the ND fillers, being about 10 times higher for the NDH sample with 2 wt.% than for the pristine PVDF in the UV region. This proves that ND particles have the ability to attenuate the transmission of UVA, UVB and UVC radiation enabling their use as UV filter ⁴⁵. In the near infrared spectral region (750-800 nm) the nanocomposites were transparent thus observing a general decrease in absorbance for almost all samples ^{12, 46}. Figure 4b shows that the absorbance (at both the wavelengths of 400 and 600 nm) increased with increasing of the nanofiller concentration, regardless the ND type, presenting an increment of about 40 % from 400 to 600 nm for the films with higher nanofillers concentration (2 wt.%). The variations of the concentration and type of ND embedded into the PVDF films enable to tune to a certain extent the optical properties of the composite samples in order to achieve specific application demands, specifically the absorption of UV radiation, which allows their use as components of sunscreens for UV radiation ⁴⁷. The films are near to transparent in the spectral regions of visible and near infrared and absorb in the UV region, providing effective protection from the UV radiation, this behavior is similar to that reported for thin films of poly(vinylpyrrolidone) with NDs ⁴⁵.

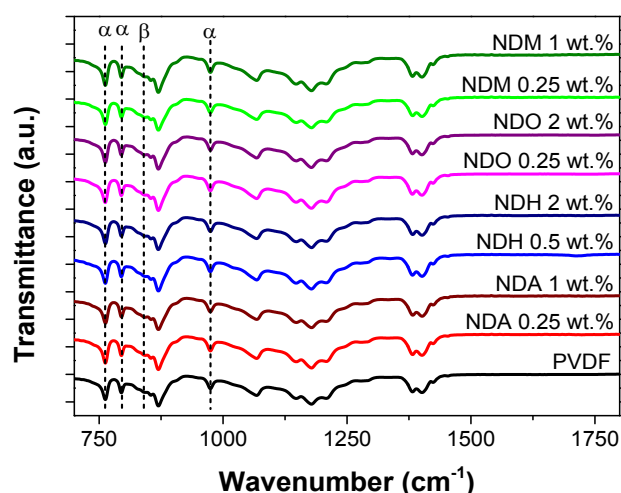


Figure 5. FTIR-ATR spectra of PVDF polymer and various ND/PVDF composites.

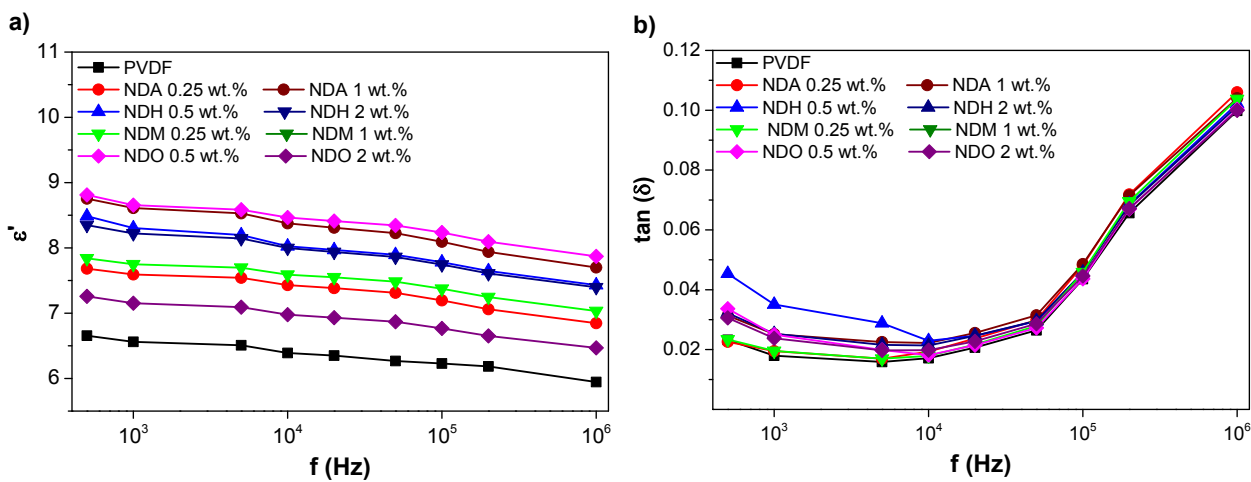
Through the FTIR-ATR spectroscopy was possible to identify the PVDF polymer phases and their relative content in the composites, which made it possible to reveal any effects of the nanofillers on the polymer crystallization. Figure 5 shows that all samples crystallized mainly in the non-polar α phase, with residual traces of the β phase. The exclusive and characteristic absorption bands of α PVDF (766, 795 and 976 cm⁻¹) were found in the spectra, what was expected considering the selected processing conditions from the melt²⁸. The α phase concentration, determined by equation 1, ranged between about 92 % and 94 % with the maximum value obtained for the sample with 0.5 wt.% of NDO. Furthermore, no traces of γ -PVDF were

1
2
3 detected. Thus, the addition of the ND fillers and the applied surface
4
5
6
7 functionalizations did not interfere in the crystallization of PVDF and did not promote
8
9
10 the nucleation of γ -PVDF, as observed in previous works with similar composites with
11
12
13 ND ¹² or with carbonaceous nanofillers ⁴⁸.
14
15
16
17

18 Figure S2 and Table T1 (supplementary information, SI) show representative
19
20
21 thermograms and the corresponding samples crystallinity. The melting temperature
22
23
24
25 (T_m) and the degree of crystallinity were determined from the DSC thermograms and
26
27
28 equation 2, respectively. All the samples present the endothermic peak at
29
30
31
32 approximately 170 °C (Figure S2, SI) ascribed to the melting of the α phase of the
33
34
35 polymer ²⁸, which is in agreement with the α phase amounts mentioned above. No
36
37
38 shifts were detected in the melting peak of the composites in comparison with the
39
40
41
42 pristine PVDF film, with the exceptions of 2 wt.% of NDM and 2 wt.% of NDO films
43
44
45 with, which exhibited a shift of approximately +2 and -2 °C, respectively. In the case
46
47
48
49 of 2 wt.% NDO, presumably larger interactions between NDs nanofillers and the
50
51
52
53 polymer matrix led to the enhancement of the composite thermal stability ⁴⁹. The
54
55
56
57 degree of crystallinity (Table T1, SI) was determined through the enthalpy of the
58
59
60

thermogram’s melting peak, and the highest value was obtained for the PVDF film with $\approx 63\%$. Considering the experimental error of 3% in the calculation of the crystallinity, the differences in the degree of crystallinity were not significant (Table T1, SI). Nevertheless, it seems that the incorporation of the nanofillers to the polymer slightly reduce the degree of crystallinity, with a minimum of $\approx 58\%$ in the case of $0.5\text{ wt.}\%$ NDA. This would suggest that the ND particles acted as defects during the crystallization process ⁴⁹, independently of the filler type or content.

Electrical properties. Figure 6 shows the dielectric response (Figures 6a and 6b), a.c (Figure 6c) and d.c (Figure 6d) electrical conductivity.



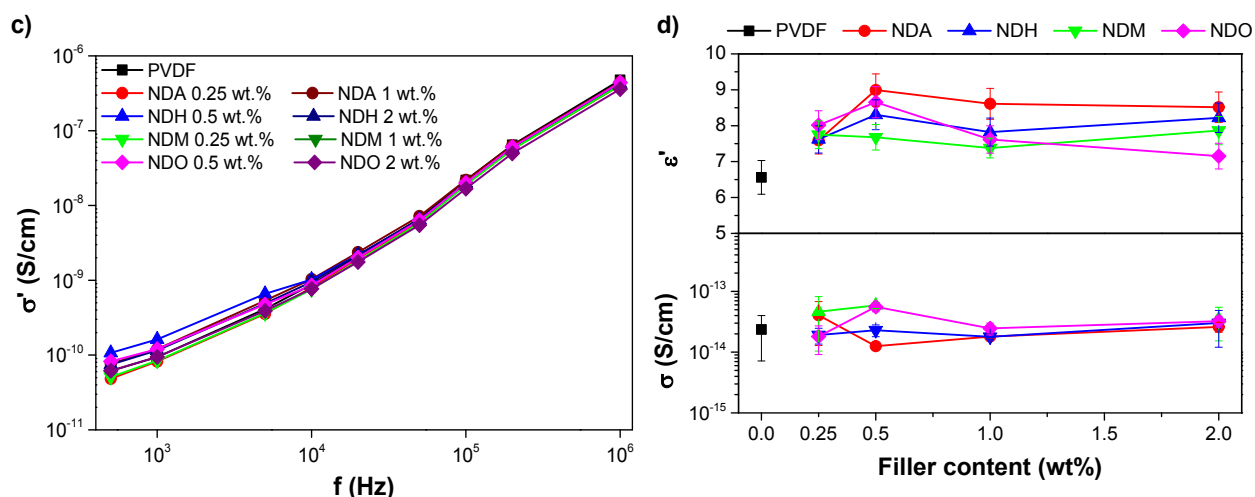


Figure 6. Electrical properties measured at room temperature: dielectric constant (a); dielectric loss (b); a.c. electrical conductivity as a function of frequency (c); dielectric constant (at 1 kHz) and d.c. conductivity as a function of filler content and type (d).

Figure 6a shows a slight decrease of the dielectric constant (ϵ') with the increase of frequency (500 Hz to 1 MHz), typical of PVDF due to the dipolar relaxation characteristics of the polymer⁵⁰. The presence of ND nanofillers did not change this dependence of ϵ' with the frequency, nonetheless a general increase of ϵ' is observed for all composite films (7–9), compared to the pristine PVDF film (6–7), similarly to that reported elsewhere for similar nanocomposites¹². Nonetheless, no relation can be established between the increase of ϵ' and the type and content of the

ND nanofillers, being most probably related to interfacial trapped charges and Maxwell-Wagner-Sillars relaxation ⁵¹, which depend on the specific characteristics of the surfaces of the different ND functionalization types. The dielectric loss tangent ($\tan(\delta)$) in the range of 500 Hz to 1 MHz is presented in Figure 6b, showing a similar frequency dependence for all samples with a maximum value of $\tan(\delta)$ of approximately 0.1 at 1 MHz. It should be noted that the relative increase of ϵ' in the composites was not accompanied by an increase in the dielectric loss, since pristine PVDF and the different composites all present similar $\tan(\delta)$, reinforcing the aforementioned behavior of the interfaces in the dielectric response. The overall behavior of the dielectric loss, in the referred frequency range, was similar for all samples, decreasing slightly up to 10^4 Hz and increasing markedly for frequencies above 10^5 Hz, typically attributed to the polymer α_a relaxation as well as to the contribution of localized charges and the crystallite/amorphous region interfaces ⁵². The a.c. conductivity (σ') in Figure 6c increased with increasing frequency with no noticeable differences between composites and pristine PVDF films meaning that the intrinsically nature of the PVDF was not modified ⁵³. The relation between ϵ' at 1 kHz and d.c. electrical conductivity (σ) with the nanofiller type and content is presented in

Figure 6d. It is shown that ϵ' (Figure 6d, top) tends to increase with the incorporation of ND nanofillers, the pristine PVDF sample presenting $\epsilon' \approx 6.5$ and the composite with 0.5 wt.% NDA displaying the maximum $\epsilon' \approx 9$. An increase of ϵ' by approximately 1.5 to 2.5 was verified in the nanocomposite samples regardless the type and the concentration of ND, whereas little significant differences were found between them. The aminated sample showed relatively higher values among the composites, with exception of the sample NDA 0.25 wt.%. The σ of the composites (Figure 6d, bottom) did not change significantly with respect to that of the pristine PVDF film; the d.c. conductivity in the same order of magnitude (10^{-14} S/cm) for all samples and the differences were within experimental errors.

Antimicrobial and antibiofilm activity. *E. coli* is responsible for a high number of infections worldwide, from mild infections such as common urinary infections to serious ones like hemorrhagic colitis, responsible for many large-scale outbreaks in recent years⁵⁴. The susceptibility of *E. coli* towards NDs was measured in culture media to assess the capability of these nanostructures alone, i.e., before being incorporated in the composite, for inhibiting the growth of bacteria. Increasing

concentrations of NDs in suspension were then put in contact with *E. coli* overnight and the optical density was measured after 24 h incubation, which is an indication of ND bacteriostatic activity. The determination of ND capability to inhibit bacterial growth comes from the knowledge that nano-scaled material has the ability to interact with the membrane of the bacterial cell due to its larger surface area, inducing high local membrane perturbation, which eventually leads to cell leakage and thus death⁵⁵⁻⁵⁶. Figure 7 shows that amine-containing NDs (NDA) possessed higher ability to prevent the *E. coli* growth, followed by the hydrogenated (NDH) and carboxylated (NDO) variants. However, non-functionalized NDs (NDM) showed no bacteriostatic activity, evidenced by a linear OD with increasing concentration which means that NDM did not affect the susceptibility of bacteria. The surficial functional groups of the NDs thus play an essential role on the antimicrobial activity of these structures. As expected, the NDs comprising amino groups, thus providing a cationic nature to the structures, are the one with higher antimicrobial activity. It has been widely proven that cationic nanostructures are able to effectively induce bacterial cell damage^{55, 57}.

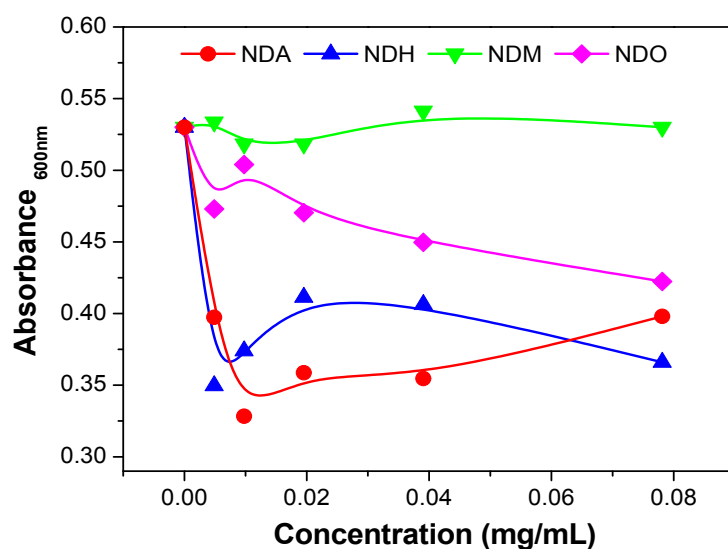


Figure 7. Dose-dependent effect of the non-functionalized and functionalized NDs in the inhibition of *E. coli* growth, measured after overnight contact with bacteria at OD at 600 nm.

Despite the fact that most of NDs in suspension show antibacterial activity, the incorporation into PVDF matrix may narrow the interaction with bacteria and the antimicrobial effect. Therefore, the corresponding PVDF composites were further tested for their antimicrobial activity. The nanocomposites comprising the highest concentration of NDs (2 wt.%) were chosen to study the effect of the addition of NDs structures to the films, not losing focus on the influence of polymer's morphology on the interaction with bacteria.

The tests were performed both at the surface of the materials through the evaluation of the total biomass and bacteria adhered to their surfaces as well as by studying the capability to induce a killing effect on the bacteria in suspension over the material. It was observed that the antimicrobial properties of the film materials were mainly confined to the surface since no CFUs reduction in suspension was observed. These results are presented in Figures 10 and 11. In Figure 8a it can be observed that the amount of *E. coli* in solution was not affected, since no relevant differences were found in terms of log reduction. This indicates that the material itself was not antimicrobial or did not leach the ND filler into the solution, which could induce bacterial death.

Nevertheless, by observing the surface of the material, analyzed with crystal violet assay (Figure 8b) and live/dead kit (Figure 9), all the nanocomposites inhibited, to a different extent, the formation of biofilm when compared to the PVDF film without any ND. The inclusion of nanodiamonds on the material surface thus influenced the capability of bacteria to adhere and form the biofilm. This is in line with previous studies that demonstrated that some specific nanostructured surfaces such as ridges,

nanopillars and grooves are able to avoid the bacteria adhesion and inhibit biofilm

formation⁵⁸⁻⁵⁹. Since the herein developed materials present a very similar

topography (Figure 2 and 3), it is proposed that the antimicrobial activity of the films

is due to the NDs themselves, that act by contact killing due to their nanosized

structure.

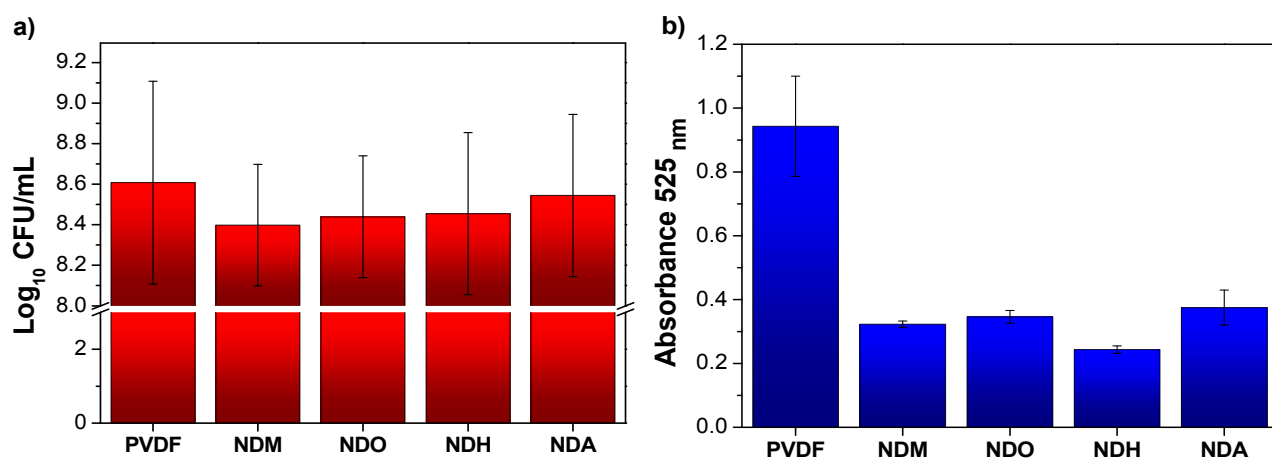


Figure 8. Antimicrobial activity of the pristine PVDF and ND/PVDF films (2 wt.%)

measured using: a) CFUs (colony forming units) of *E. coli* growing in suspension over

the nanocomposites and b) the total biomass growing on material's surface assessed

by crystal violet assay.

Figure 9 clearly shows that the *E. coli* cells adhered to the PVDF surface, most of the cells staining green, indicating a high level of bacterial viability, and to a lesser extent the NDM nanocomposite material, at higher content. On the other composite materials, besides having less cell density on the surface, they were mainly dead (represented in red), with the highest number of dead cells found over the NDH and NDA containing composites. These results corroborate with the results shown in Figure 7 where these functionalized NDs were found to induce more bacteriostatic activity.

With respect to the possible mechanism of action of the NDs, it can be hypothesized that NDs are able to kill bacteria through contact killing mechanism through the interaction with nanosized clusters that disrupt cell membrane. It has been reported that specific nanostructures, mainly positively charged ones, has the ability to interact with the bacterial cell membrane due to its larger surface area, inducing high local membrane perturbation, which eventually leads to cell leakage and thus death^{55, 60}. In fact, cationic biocides and surfactants (e.g. quaternary ammonium compounds), both possessing positively charged moieties were reported to impart bactericidal properties for a wide range of bacteria⁶¹⁻⁶².

It could thus be concluded that these NDs acted by contact killing and were not leached from the material. Thus, the developed composites can be used as antimicrobial coatings, being the NDA and NDH enriched composites particularly suitable for this application. Moreover, the polymer matrix enables green chemistry approaches⁶³ during processing, including additive manufacturing technologies⁶⁴.

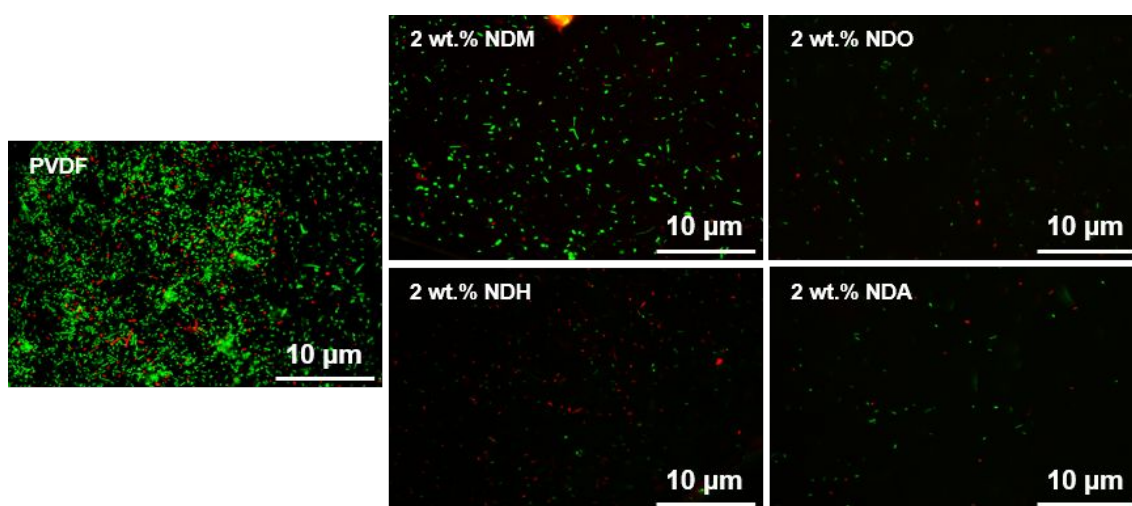


Figure 9. Fluorescence microscopy live/dead images of 24 h grown *E. coli* bacteria incubated over the nanocomposites and PVDF as a control (live cells in green and dead cells in red).

CONCLUSIONS

ND/PVDF composites were processed by solvent casting using ND fillers of four different types of surface functionalization (i.e., non-functionalized (NDM), aminated (NDA), hydrogenated (NDH) and carboxylated (NDO)) and concentrations (0.25, 0.5, 1 and 2 wt.%).

The samples show homogeneous surface morphology and regular dispersion of ND fillers along the PVDF for all composites, while the overall surface topography was similar between composites and pristine PVDF sample. The contact angle was therefore very similar among the samples, slightly increasing with the increase of NDs concentration in the PVDF matrix.

As compared to the pristine PVDF film, composite films showed up to 10 times higher absorbance in the UV region and about 40 % higher absorbance in the visual light region (i.e., at 400 and 600 nm) in the case of the NDH sample 2 wt.%. All films crystallized in the α PVDF phase (92 to 94 %), with smaller traces β PVDF, so the filler type or filler did not affect the α phase crystallization of PVDF. The dielectric constant (ϵ') of the composite films increased with about 2 with the incorporation of ND and the dielectric loss ($\tan(\delta)$) remained almost constant. The inclusion of ND

imparted antibiofilm properties to the films, with the type of ND functionalization being an essential factor to kill the bacterial cells through contact killing. NDH and NDA containing composites induced improved bactericidal activity when compared to NDM and NDO, most probably due to the effective interaction with the membrane of the bacterial cell. In short, the incorporation of several ND fillers into PVDF enables to tune the optical properties of the nanocomposites, increases the dielectric constant while not affecting the dielectric loss, and successfully imparts antimicrobial properties to the films without relevant modification of the characteristics of PVDF. These composites represent promising candidates to produce functional coatings and sensors, due to the outstanding properties of the polymer, including through additive manufacturing processes.

ASSOCIATED CONTENT

Supporting Information

Water contact angle (Figure S1);

DSC thermograms (Figure S2);

Degree of crystallinity (Table T1).

AUTHOR INFORMATION

Corresponding Author

* j.nunespereira@ubi.pt; ORCID: 0000-0002-6024-8716

* senentxu.lanceros@bcmaterials.net; ORCID: 0000-0001-6791-7620

Funding Sources

Fundação para a Ciência e a Tecnologia (FCT);

Fundo Social Europeu (FSE);

Programa Operacional Regional Centro 2020, Norte 2020 and Lisboa 2020;

Dutch Research Council (NOW),

Spanish State Research Agency (AEI);

European Regional Development Fund (ERFD);

Basque Government Industry and Education Departments.

Author Contributions

The manuscript was written through contributions of all authors. All authors have given approval to the final version of the manuscript.

ACKNOWLEDGEMENTS

The authors thank the Fundação para a Ciência e a Tecnologia (FCT), Fundo Social Europeu (FSE) and Programa Operacional Regional Centro 2020, Norte 2020 and Lisboa 2020 for the Strategic Funding UID/EMS/00151/2020 and UID/FIS/04650/2020, projects PTDC/BTM-MAT/28237/2017 and PTDC/EMD-EMD/28159/2017, and the grants SFRH/BPD/117838/2016 (J.N.P.), SFRH/BPD/110914/2015 (P.C.), SFRH/BD/145345/2019 (L.F.),

SFRH/BD/145455/2019 (E.O.C.), SFRH/BPD/121464/2016 (M.M.F.) and Associate Laboratory for Green Chemistry—LAQV which is financed by national funds from FCT/MCTES (UIDB/50006/2020). J.G.B. thanks the Dutch Research Council (NWO) for funding as part of the Open Technology Programme (project no. 16361). Financial support from the Spanish State Research Agency (AEI) and the European Regional Development Fund (ERFD) through the project PID2019-106099RB-C43 / AEI / 10.13039/501100011033 and from the Basque Government Industry and Education Departments under the ELKARTEK, HAZITEK and PIBA (PIBA-2018-06) programs is also acknowledged. The authors thank Dr. Carlos Sá (CEMUP) for assistance with the XPS analyses.

ABBREVIATIONS

ATCC, American Type Culture Collection; AFM, atomic force microscopy; BE, binding energy; CFU, colony forming units; DCS, differential scanning calorimetry; DMF, N,N-dimethylformamide; *E. coli*, *Escherichia coli*; FAT, fixed analyzer

transmission; FTIR, Fourier-transform infrared spectroscopy; NB, Nutrient Broth;

NDA, uDiamond® Amine; NDH, uDiamond® Hydrogen P; NDM, Carbodeon

uDiamond® Molto; NDO, uDiamond® VOX P; NDPC, phospholipid ND compound;

NDs, nanodiamonds; OD, optical density; PBS, phosphate buffer solution; PLGA,

poly(lactic-co-glycolic acid); PVDF, poly(vinylidene fluoride); SD, standard deviation;

SEM, scanning electron microscopy; XPS, X-ray photoelectron spectroscopy.

REFERENCES

- (1) Yu, J.; Qian, R.; Jiang, P. Enhanced thermal conductivity for PVDF composites with a hybrid functionalized graphene sheet-nanodiamond filler. *Fibers and Polymers* **2013**, *14* (8), 1317-1323, DOI: <https://doi.org/10.1007/s12221-013-1317-7>.
- (2) Prasad, K. E.; Das, B.; Maitra, U.; Ramamurty, U.; Rao, C. N. R. Extraordinary synergy in the mechanical properties of polymer matrix composites reinforced with 2 nanocarbons. *Proceedings of the National Academy of Sciences* **2009**, *106* (32), 13186-13189, DOI: <https://doi.org/10.1073/pnas.0905844106>.
- (3) Martins, P.; Nunes, J. S.; Oliveira, J.; Peřinka, N.; Lanceros-Mendez, S. Spray-printed magnetoelectric multifunctional composites. *Composites Part B: Engineering* **2020**, *187*, 107829, DOI: <https://doi.org/10.1016/j.compositesb.2020.107829>.
- (4) Li, E.; Ye, P.; Kang, J.; Yin, C.; Cheng, F. Facile fabrication of photochromic microspheres with multimodal hierarchically porous for selective extraction of lithium ions. *Materials Letters* **2020**, *270*, 12670, DOI: <https://doi.org/10.1016/j.matlet.2020.127670>.
- (5) Correia, D. M.; Nunes-Pereira, J.; Alikin, D.; Kholkin, A. L.; Carabineiro, S. A. C.; Rebouta, L.; Rodrigues, M. S.; Vaz, F.; Costa, C. M.; Lanceros-Méndez, S. Surface wettability modification of poly(vinylidene fluoride) and copolymer films and membranes by plasma treatment. *Polymer* **2019**, *169*, 138-147, DOI: <https://doi.org/10.1016/j.polymer.2019.02.042>.
- (6) Zhang, Z.-Q.; Zeng, R.-C.; Lin, C.-G.; Wang, L.; Chen, X.-B.; Chen, D.-C. Corrosion resistance of self-cleaning silane/polypropylene composite coatings on magnesium alloy AZ31. *Journal of Materials Science & Technology* **2020**, *41*, 43-55, DOI: <https://doi.org/10.1016/j.jmst.2019.08.056>.

- (7) Ojogbo, E.; Ward, V.; Mekonnen, T. H. Functionalized starch microparticles for contact-active antimicrobial polymer surfaces. *Carbohydrate Polymers* **2020**, *229*, 115422, DOI: <https://doi.org/10.1016/j.carbpol.2019.115422>.
- (8) Mochalin, V. N.; Shenderova, O.; Ho, D.; Gogotsi, Y. The properties and applications of nanodiamonds. *Nat Nano* **2012**, *7* (1), 11-23, DOI: <https://doi.org/10.1038/nnano.2011.209>.
- (9) Meinhardt, T.; Lang, D.; Dill, H.; Krueger, A. Pushing the functionality of diamond nanoparticles to new horizons: Orthogonally functionalized nanodiamond using click chemistry. *Advanced Functional Materials* **2011**, *21* (3), 494-500, DOI: <https://doi.org/10.1002/adfm.201001219>.
- (10) Zhang, Y.; Choi, J. R.; Park, S.-J. Thermal conductivity and thermo-physical properties of nanodiamond-attached exfoliated hexagonal boron nitride/epoxy nanocomposites for microelectronics. *Composites Part A: Applied Science and Manufacturing* **2017**, *101*, 227-236, DOI: <http://dx.doi.org/10.1016/j.compositesa.2017.06.019>.
- (11) Zhang, Y.; Rhee, K. Y.; Hui, D.; Park, S.-J. A critical review of nanodiamond based nanocomposites: Synthesis, properties and applications. *Composites Part B: Engineering* **2018**, *143*, 19-27, DOI: <https://doi.org/10.1016/j.compositesb.2018.01.028>.
- (12) Nunes-Pereira, J.; Silva, A. R.; Ribeiro, C.; Carabineiro, S. A. C.; Buijnsters, J. G.; Lanceros-Méndez, S. Nanodiamonds/poly(vinylidene fluoride) composites for tissue engineering applications. *Composites Part B: Engineering* **2017**, *111*, 37-44, DOI: <https://doi.org/10.1016/j.compositesb.2016.12.014>.
- (13) Al-Jumaili, A.; Alancherry, S.; Bazaka, K.; Jacob, M. V. Review on the antimicrobial properties of carbon nanostructures. *Materials (Basel)* **2017**, *10* (9), 1066, DOI: <https://doi.org/10.3390/ma10091066>.
- (14) Szunerits, S.; Barras, A.; Boukherroub, R. Antibacterial applications of nanodiamonds. *Int J Environ Res Public Health* **2016**, *13* (4), 413-413, DOI: <https://doi.org/10.3390/ijerph13040413>.
- (15) Wilks, S. A.; Michels, H.; Keevil, C. W. The survival of *Escherichia coli* O157 on a range of metal surfaces. *International Journal of Food Microbiology* **2005**, *105* (3), 445-454, DOI: <https://doi.org/10.1016/j.ijfoodmicro.2005.04.021>.
- (16) Liao, S. Y.; Read, D. C.; Pugh, W. J.; Furr, J. R.; Russell, A. D. Interaction of silver nitrate with readily identifiable groups: relationship to the antibacterial action of silver ions. *Letters in Applied Microbiology* **2003**, *25* (4), 279-283, DOI: <http://dx.doi.org/10.1046/j.1472-765X.1997.00219.x>.
- (17) Ioannou, C. J.; Hanlon, G. W.; Denyer, S. P. Action of disinfectant quaternary ammonium compounds against staphylococcus aureus. *Antimicrobial Agents and Chemotherapy* **2006**, *51* (1), 296-306, DOI: <https://doi.org/10.1128/AAC.00375-06>.
- (18) Mao, B.-H.; Chen, Z.-Y.; Wang, Y.-J.; Yan, S.-J. Silver nanoparticles have lethal and sublethal adverse effects on development and longevity by inducing ROS-mediated stress responses. *Scientific Reports* **2018**, *8* (1), 2445, DOI: <https://doi.org/10.1038/s41598-018-20728-z>.
- (19) Bumgardner, J. D.; Lucas, L. C.; Tilden, A. B. Toxicity of copper-based dental alloys in cell culture. *J Biomed Mater Res* **1989**, *23* (10), 1103-1114, DOI: <https://doi.org/10.1002/jbm.820231002>.
- (20) Fouda, S. M.; Gad, M. M.; Ellakany, P.; Al-Thobity, A. M.; Al-Harbi, F. A.; Virtanen, J. I.; Raustia, A. The effect of nanodiamonds on candida albicans adhesion and surface characteristics of PMMA denture base material - an in vitro study. *J Appl Oral Sci* **2019**, *27*, e20180779-e20180779, DOI: <https://doi.org/10.1590/1678-7757-2018-0779>.
- (21) Chen, M.; Pierstorff, E. D.; Lam, R.; Li, S.-Y.; Huang, H.; Osawa, E.; Ho, D. Nanodiamond-mediated delivery of water-insoluble therapeutics. *ACS Nano* **2009**, *3* (7), 2016-2022, DOI: <https://doi.org/10.1021/nn900480m>.

- (22) Lim, D. G.; Jung, J. H.; Ko, H. W.; Kang, E.; Jeong, S. H. Paclitaxel–nanodiamond nanocomplexes enhance aqueous dispersibility and drug retention in cells. *ACS Applied Materials & Interfaces* **2016**, *8* (36), 23558-23567, DOI: <http://dx.doi.org/10.1021/acsami.6b08079>.
- (23) Giammarco, J.; Mochalin, V. N.; Haeckel, J.; Gogotsi, Y. The adsorption of tetracycline and vancomycin onto nanodiamond with controlled release. *Journal of Colloid and Interface Science* **2016**, *468*, 253-261, DOI: <http://dx.doi.org/10.1016/j.jcis.2016.01.062>.
- (24) Toh, T.-B.; Lee, D.-K.; Hou, W.; Abdullah, L. N.; Nguyen, J.; Ho, D.; Chow, E. K.-H. Nanodiamond–mitoxantrone complexes enhance drug retention in chemoresistant breast cancer cells. *Molecular Pharmaceutics* **2014**, *11* (8), 2683-2691, DOI: <http://dx.doi.org/10.1021/mp5001108>.
- (25) Zhang, F.; Song, Q.; Huang, X.; Li, F.; Wang, K.; Tang, Y.; Hou, C.; Shen, H. A novel high mechanical property PLGA composite matrix loaded with nanodiamond–phospholipid compound for bone tissue engineering. *ACS Applied Materials & Interfaces* **2016**, *8* (2), 1087-1097, DOI: <https://doi.org/10.1021/acsami.5b09394>.
- (26) Simioni, N. B.; Silva, T. A.; Oliveira, G. G.; Fatibello-Filho, O. A nanodiamond-based electrochemical sensor for the determination of pyrazinamide antibiotic. *Sensors and Actuators B: Chemical* **2017**, *250*, 315-323, DOI: <http://dx.doi.org/10.1016/j.snb.2017.04.175>.
- (27) Schrand, A. M.; Hens, S. A. C.; Shenderova, O. A. Nanodiamond particles: properties and perspectives for bioapplications. *Critical Reviews in Solid State and Materials Sciences* **2009**, *34* (1-2), 18-74, DOI: <https://doi.org/10.1080/10408430902831987>.
- (28) Martins, P.; Lopes, A. C.; Lanceros-Mendez, S. Electroactive phases of poly(vinylidene fluoride): Determination, processing and applications. *Progress in Polymer Science* **2014**, *39* (4), 683-706, DOI: <https://doi.org/10.1016/j.progpolymsci.2013.07.006>.
- (29) Ribeiro, C.; Costa, C. M.; Correia, D. M.; Nunes-Pereira, J.; Oliveira, J.; Martins, P.; Gonçalves, R.; Cardoso, V. F.; Lanceros-Méndez, S. Electroactive poly(vinylidene fluoride)-based structures for advanced applications. *Nature Protocols* **2018**, *13* (4), 681-704, DOI: <https://doi.org/10.1038/nprot.2017.157>.
- (30) Carvalho, E. O.; Fernandes, M. M.; Padrao, J.; Nicolau, A.; Marqués-Marchán, J.; Asenjo, A.; Gama, F. M.; Ribeiro, C.; Lanceros-Mendez, S. Tailoring bacteria response by piezoelectric stimulation. *ACS Applied Materials & Interfaces* **2019**, *11* (30), 27297-27305, DOI: <https://doi.org/10.1021/acsami.9b05013>.
- (31) Mendes-Felipe, C.; Oliveira, J.; Etxebarria, I.; Vilas-Vilela, J. L.; Lanceros-Mendez, S. State-of-the-art and future challenges of UV curable polymer-based smart materials for printing technologies. *Advanced Materials Technologies* **2019**, *4* (3), 1800618, DOI: <https://doi.org/10.1002/admt.201800618>.
- (32) Fu, Y.; Yang, Q.; Xu, M.; Kong, H.; Chen, H.; Fu, Y.; Yao, Y.; Zhou, H.; Zhou, J. Secondary bacterial infections in critical ill patients with coronavirus disease 2019. *Open Forum Infectious Diseases* **2020**, *7* (6), DOI: <https://doi.org/10.1093/ofid/ofaa220>.
- (33) Benz, M.; Euler, W. B. Determination of the crystalline phases of poly(vinylidene fluoride) under different preparation conditions using differential scanning calorimetry and infrared spectroscopy. *Journal of Applied Polymer Science* **2003**, *89* (4), 1093-1100, DOI: <https://doi.org/10.1002/app.12267>.
- (34) Holt, K. B.; Caruana, D. J.; Millán-Barrios, E. J. Electrochemistry of undoped diamond nanoparticles: Accessing surface redox states. *Journal of the American Chemical Society* **2009**, *131* (32), 11272-11273, DOI: <https://doi.org/10.1021/ja902216n>.
- (35) Pastrana-Martínez, L. M.; Morales-Torres, S.; Carabineiro, S. A. C.; Buijnsters, J. G.; Faria, J. L.; Figueiredo, J. L.; Silva, A. M. T. Nanodiamond-TiO₂ composites for heterogeneous photocatalysis. *ChemPlusChem* **2013**, *78* (8), 801-807, DOI: <https://doi.org/10.1002/cplu.201300094>.

- (36) Valerii Yu, D. Detonation-synthesis nanodiamonds: synthesis, structure, properties and applications. *Russian Chemical Reviews* **2007**, 76 (4), 339, DOI: <https://doi.org/10.1070/RC2007v076n04ABEH003643>.
- (37) Jansen, R. J. J.; van Bekkum, H. XPS of nitrogen-containing functional groups on activated carbon. *Carbon* **1995**, 33 (8), 1021-1027, DOI: [http://dx.doi.org/10.1016/0008-6223\(95\)00030-H](http://dx.doi.org/10.1016/0008-6223(95)00030-H).
- (38) Duan, X.; Ao, Z.; Li, D.; Sun, H.; Zhou, L.; Suvorova, A.; Saunders, M.; Wang, G.; Wang, S. Surface-tailored nanodiamonds as excellent metal-free catalysts for organic oxidation. *Carbon* **2016**, 103, 404-411, DOI: <https://doi.org/10.1016/j.carbon.2016.03.034>.
- (39) Jiang, T.; Xu, K. FTIR study of ultradispersed diamond powder synthesized by explosive detonation. *Carbon* **1995**, 33 (12), 1663-1671, DOI: [http://dx.doi.org/10.1016/0008-6223\(95\)00115-1](http://dx.doi.org/10.1016/0008-6223(95)00115-1).
- (40) Kuznetsov, V. L.; Aleksandrov, M. N.; Zagoruiko, I. V.; Chuvilin, A. L.; Moroz, E. M.; Kolomiichuk, V. N.; Likholobov, V. A.; Brylyakov, P. M.; Sakovitch, G. V. Study of ultradispersed diamond powders obtained using explosion energy. *Carbon* **1991**, 29 (4), 665-668, DOI: [http://dx.doi.org/10.1016/0008-6223\(91\)90135-6](http://dx.doi.org/10.1016/0008-6223(91)90135-6).
- (41) Mironov, E.; Koretz, A.; Petrov, E. Detonation synthesis ultradispersed diamond structural properties investigation by infrared absorption. *Diamond and Related Materials* **2002**, 11 (3-6), 872-876, DOI: [https://doi.org/10.1016/S0925-9635\(01\)00723-3](https://doi.org/10.1016/S0925-9635(01)00723-3).
- (42) Kirmani, A. R.; Peng, W.; Mahfouz, R.; Amassian, A.; Losovyj, Y.; Idriss, H.; Katsiev, K. On the relation between chemical composition and optical properties of detonation nanodiamonds. *Carbon* **2015**, 94, 79-84, DOI: <https://doi.org/10.1016/j.carbon.2015.06.038>.
- (43) Mendes, S. F.; Costa, C. M.; Caparros, C.; Sencadas, V.; Lanceros-Méndez, S. Effect of filler size and concentration on the structure and properties of poly(vinylidene fluoride)/BaTiO₃ nanocomposites. *Journal of Materials Science* **2012**, 47 (3), 1378-1388, DOI: <https://doi.org/10.1007/s10853-011-5916-7>.
- (44) Prajitno, D. H.; Maulana, A.; Syarif, D. G. Effect of surface roughness on contact angle measurement of nanofluid on surface of stainless steel 304 by sessile drop method. *Journal of Physics: Conference Series* **2016**, 739, 012029, DOI: <https://doi.org/10.1088/1742-6596/739/1/012029>.
- (45) Attia, N. F.; Rao, J. P.; Geckeler, K. E. Nanodiamond-polymer nanoparticle composites and their thin films. *Journal of Nanoparticle Research* **2014**, 16 (4), 2361, DOI: <https://doi.org/10.1007/s11051-014-2361-y>.
- (46) Papagiannouli, I.; Bourlinos, A. B.; Bakandritsos, A.; Couris, S. Nonlinear optical properties of colloidal carbon nanoparticles: nanodiamonds and carbon dots. *RSC Advances* **2014**, 4 (76), 40152-40160, DOI: <http://dx.doi.org/10.1039/C4RA04714A>.
- (47) Wu, M.-S.; Sun, D.-S.; Lin, Y.-C.; Cheng, C.-L.; Hung, S.-C.; Chen, P.-K.; Yang, J.-H.; Chang, H.-H. Nanodiamonds protect skin from ultraviolet B-induced damage in mice. *Journal of Nanobiotechnology* **2015**, 13 (1), 35, DOI: <https://doi.org/10.1186/s12951-015-0094-4>.
- (48) Nunes-Pereira, J.; Sharma, P.; Fernandes, L. C.; Oliveira, J.; Moreira, J. A.; Sharma, R. K.; Lanceros-Mendez, S. Poly(vinylidene fluoride) composites with carbon nanotubes decorated with metal nanoparticles. *Composites Part B: Engineering* **2018**, 142, 1-8, DOI: <https://doi.org/10.1016/j.compositesb.2017.12.047>.
- (49) Martins, P.; Costa, C. M.; Lanceros-Mendez, S. Nucleation of electroactive β -phase poly(vinylidene fluoride) with CoFe₂O₄ and NiFe₂O₄ nanofillers: a new method for the preparation of multiferroic nanocomposites. *Applied Physics A* **2011**, 103 (1), 233-237, DOI: <http://dx.doi.org/10.1007/s00339-010-6003-7>.
- (50) Sousa, R. E.; Nunes-Pereira, J.; Ferreira, J. C. C.; Costa, C. M.; Machado, A. V.; Silva, M. M.; Lanceros-Mendez, S. Microstructural variations of poly(vinylidene fluoride co-hexafluoropropylene) and their influence on the thermal, dielectric and piezoelectric properties.

- Polymer Testing* **2014**, *40*, 245-255, DOI: <http://dx.doi.org/10.1016/j.polymertesting.2014.09.012>.
- (51) Lopes, A. C.; Costa, C. M.; Serra, R. S. i.; Neves, I. C.; Ribelles, J. L. G.; Lanceros-Méndez, S. Dielectric relaxation, ac conductivity and electric modulus in poly(vinylidene fluoride)/NaY zeolite composites. *Solid State Ionics* **2013**, *235*, 42-50, DOI: <https://doi.org/10.1016/j.ssi.2013.01.013>.
- (52) Sasabe, H.; Saito, S.; Asahina, M.; Kakutani, H. Dielectric relaxations in poly(vinylidene fluoride). *Journal of Polymer Science Part A-2: Polymer Physics* **1969**, *7* (8), 1405-1414, DOI: <http://dx.doi.org/10.1002/pol.1969.160070810>.
- (53) Carabineiro, S. A. C.; Thavorn-Amornsri, T.; Pereira, M. F. R.; Serp, P.; Figueiredo, J. L. Comparison between activated carbon, carbon xerogel and carbon nanotubes for the adsorption of the antibiotic ciprofloxacin. *Catalysis Today* **2012**, *186* (1), 29-34, DOI: <https://doi.org/10.1016/j.cattod.2011.08.020>.
- (54) Allocati, N.; Masulli, M.; Alexeyev, M. F.; Di Ilio, C. *Escherichia coli* in Europe: an overview. *Int J Environ Res Public Health* **2013**, *10* (12), 6235-6254, DOI: <https://doi.org/10.3390/ijerph10126235>.
- (55) Fernandes, M. M.; Francesko, A.; Torrent-Burgués, J.; Carrión-Fité, F. J.; Heinze, T.; Tzanov, T. Sonochemically processed cationic nanocapsules: Efficient antimicrobials with membrane disturbing capacity. *Biomacromolecules* **2014**, *15* (4), 1365-1374, DOI: <https://doi.org/10.1021/bm4018947>.
- (56) Fernandes, M. M.; Ivanova, K.; Hoyo, J.; Pérez-Rafael, S.; Francesko, A.; Tzanov, T. Nanotransformation of vancomycin overcomes the intrinsic resistance of Gram-negative bacteria. *ACS Applied Materials & Interfaces* **2017**, *9* (17), 15022-15030, DOI: <https://doi.org/10.1021/acsami.7b00217>.
- (57) Liu, L.; Xu, K.; Wang, H.; Jeremy Tan, P. K.; Fan, W.; Venkatraman, S. S.; Li, L.; Yang, Y.-Y. Self-assembled cationic peptide nanoparticles as an efficient antimicrobial agent. *Nature Nanotechnology* **2009**, *4* (7), 457-463, DOI: <https://doi.org/10.1038/nnano.2009.153>.
- (58) Hasan, J.; Crawford, R.; Ivanova, E. Antibacterial surfaces: The quest for a new generation of biomaterials. *Trends in biotechnology* **2013**, *31*, DOI: <https://doi.org/10.1016/j.tibtech.2013.01.017>.
- (59) Hasan, J.; Chatterjee, K. Recent advances in engineering topography mediated antibacterial surfaces. *Nanoscale* **2015**, *7* (38), 15568-15575, DOI: <http://dx.doi.org/10.1039/C5NR04156B>.
- (60) Zhou, C.; Wang, F.; Chen, H.; Li, M.; Qiao, F.; Liu, Z.; Hou, Y.; Wu, C.; Fan, Y.; Liu, L.; Wang, S.; Wang, Y. Selective antimicrobial activities and action mechanism of micelles self-assembled by cationic oligomeric surfactants. *ACS Applied Materials & Interfaces* **2016**, *8* (6), 4242-4249, DOI: <https://doi.org/10.1021/acsami.5b12688>.
- (61) Blesic, M.; Marques, M. H.; Plechkova, N. V.; Seddon, K. R.; Rebelo, L. P. N.; Lopes, A. Self-aggregation of ionic liquids: micelle formation in aqueous solution. *Green Chemistry* **2007**, *9* (5), 481-490, DOI: <http://dx.doi.org/10.1039/B615406A>.
- (62) Jungnickel, C.; Łuczak, J.; Ranke, J.; Fernández, J. F.; Müller, A.; Thöming, J. Micelle formation of imidazolium ionic liquids in aqueous solution. *Colloids and Surfaces A: Physicochemical and Engineering Aspects* **2008**, *316* (1), 278-284, DOI: <https://doi.org/10.1016/j.colsurfa.2007.09.020>.
- (63) Nunes-Pereira, J.; Martins, P.; Cardoso, V. F.; Costa, C. M.; Lanceros-Méndez, S. A green solvent strategy for the development of piezoelectric poly(vinylidene fluoride–trifluoroethylene) films for sensors and actuators applications. *Materials & Design* **2016**, *104*, 183-189, DOI: <https://doi.org/10.1016/j.matdes.2016.05.023>.

1
2
3
4
5
6
7
8
9
10
11
12
13
14
15
16
17
18
19
20
21
22
23
24
25
26
27
28
29
30
31
32
33
34
35
36
37
38
39
40
41
42
43
44
45
46
47
48
49
50
51
52
53
54
55
56
57
58
59
60

(64) Oliveira, J.; Correia, V.; Castro, H.; Martins, P.; Lanceros-Mendez, S. Polymer-based smart materials by printing technologies: Improving application and integration. *Additive Manufacturing* **2018**, *21*, 269-283, DOI: <https://doi.org/10.1016/j.addma.2018.03.012>.

TABLE OF CONTENTS GRAPHIC

